

Thermally activated processes in polymer dynamics

Lorenzo Bongini⁽¹⁾, Roberto Livi^{(2),(1)}, Antonio Politi^{(3),(1)}, and Alessandro Torcini^{(3),(1)}

(1) *INFN, UdR Firenze, via Sansone, 1 - I-50019 Sesto Fiorentino, Italy*

(2) *Dipartimento di Fisica, Università di Firenze, via Sansone, 1 - I-50019 Sesto Fiorentino, Italy*

(3) *Istituto Nazionale di Ottica Applicata, L.go E. Fermi, 6 - I-50125 Firenze, Italy*

(Dated: November 6, 2018)

Jumps between neighboring minima in the energy landscape of both homopolymeric and heteropolymeric chains are numerically investigated by determining the average escape time from different valleys. The numerical results are compared to the theoretical expression derived by Langer [J.S. Langer, *Ann. Phys.* **54** (1969) 258] with reference to a $2N$ -dimensional space. Our simulations indicate that the dynamics within the native valley is well described by a sequence of thermally activated process up to temperatures well above the folding temperature. At larger temperatures, systematic deviations from the Langer's estimate are instead observed. Several sources for such discrepancies are thoroughly discussed.

PACS numbers: 05.40.-a,05.10.Gg,05.20.Dd,87.15.Cc,82.37.-j

I. INTRODUCTION

Polymeric chains exhibit quite a rich variety of dynamical properties. At high temperatures, kinetic energy is large enough to allow a chain exploring most of the accessible phase-space. In this regime, the polymer typically assumes a “random coil” structure. At intermediate temperatures, internal forces and the interaction with the solvent become strong enough to stabilize compact configurations [1]. However, kinetic energy fluctuations are still able to drive the chain from one to another minimum of the energy landscape. The properties of this itinerant dynamics depend on several factors: the height of the barriers separating neighboring minima, their accessibility and, more generally, the overall structure of the energy landscape. Upon further decreasing the temperature, a heteropolymer typically undergoes a glass transition and may freeze in one of several distinct free-energy minima. Only some peculiar heteropolymers exhibit a transition to a “folding regime”, i.e. are characterized by a relatively fast convergence towards the absolute energy minimum, irrespectively of the initial state. In this case, the heteropolymer is said to be a “good folder” and it can be viewed as a specimen of a protein, that always evolves to its native configuration (NC) [2].

Independently whether a given polymer is homogeneous or heterogeneous, whether it is a good or a bad folder, a complete understanding of its dynamical properties passes through the description of the jump processes between different energy valleys [3, 4]. Free-energy valleys are indeed collections of distinct minima and studying the connectivity of such minima can help identifying and parametrizing the relevant macroscopic states [5, 6]. In the hope to eventually make substantial progress along this line, in this paper we aim at testing the validity of the expressions utilized to characterize the single escape processes. In the current literature, the escape is often viewed as an activation process and Kramers-like formulae, derived for low-dimensional systems, are applied to characterize high-dimensional systems without testing their validity. In this paper we present a detailed check of the formula derived by Langer in 1969 [7], finding that the escape process is strongly influenced by the entropic contribution associated with the local geometry of the energy landscape.

In Sec. 2 we introduce the polymer model used as a testing ground for the numerical analysis of activation processes in relatively high-dimensional systems [8]. It consists of a chain of two types of beads embedded in a two-dimensional space. In the same section, we briefly recall the relevant properties of both homogeneous and heterogeneous systems upon varying the temperature. In Sec. 3, the general theoretical ideas lying behind the derivation of Langer's formula are briefly summarized. The technical difficulties associated with the determination of geometrical factors are also discussed together with some possible approximation schemes. In Section 4, theoretical predictions are compared with numerical simulations for specimens of bad and good folders. In spite of an overall qualitative agreement, systematic deviations are found at relatively high temperatures, the origin of which is discussed in Sec. 5, where several effects are separately discussed. Finally, in Sec. 6, the main conclusions are summarized and the open problems briefly recalled.

II. THE MODEL: DEFINITIONS AND THERMODYNAMICAL PROPERTIES

In this paper we study the escape process from an energy valley with reference to a model thoroughly investigated in [9], where the authors slightly modified a previous version, originally introduced in [8]. The model, designed to simulate sequences of amino acids interacting within a solvent, describes a chain of L monomers embedded in a 2-dimensional space. At variance with [8], where monomers were rigidly linked along the backbone, in [9] a nearest-neighbor harmonic potential was instead assumed,

$$V_1(r_{i,i+1}) = \alpha(r_{i,i+1} - r_0)^2, \quad (1)$$

where $r_{i,j} = \sqrt{(x_i - x_j)^2 + (y_i - y_j)^2}$ is the distance between the i th and the j -th monomer, while x_i, y_i are the coordinates of the i th monomer. Without loss of generality, the equilibrium distance r_0 is set equal to 1, while the interaction constant α has been fixed equal to 20 so as to induce an almost rigid interaction between neighbouring monomers [10].

The second term expresses the energy cost of local bending; it is described by the three-body interaction term

$$V_2(\theta_i) = \frac{1 - \cos \theta_i}{16} \quad (2)$$

where θ_i is the angle formed between the links connecting the $(i-1)$ -st, the i -th and the $(i+1)$ -st monomers. In particular,

$$\cos \theta_i = \frac{(x_i - x_{i-1})(x_{i+1} - x_i) + (y_i - y_{i-1})(y_{i+1} - y_i)}{r_{i,i-1}r_{i+1,i}}, \quad (3)$$

where $-\pi < \theta_i < \pi$.

Finally, heterogeneity is ensured by Lennard-Jones type interaction between non-neighbouring monomers ($|i-j| > 1$)

$$V_3(r_{i,j}) = \frac{1}{r_{i,j}^{12}} - \frac{c_{i,j}}{r_{i,j}^6} \quad (4)$$

where

$$c_{i,j} = \frac{1}{2}(2 - 3\xi_i - 3\xi_j + 5\xi_i\xi_j) \quad .$$

and $\xi_i = 0$ indicates that the i th monomer is hydrophobic (H), while $\xi_i = 1$ corresponds to a polar (P) one. As a result, the interaction is attractive if the two monomers are either both hydrophobic or both polar ($c_{i,j} = 1$ and $1/2$, respectively), while it is repulsive, if the monomers belong to different species (in which case $c_{i,j} = -1/2$). This potential choice simulates the effective interaction among H and P monomers in the presence of a solvent. In fact, since H monomers prefer to avoid a direct contact with the solvent, they tend to clusterize in the interior where they can be shielded from water by a shell of P monomers. The net result is an effective H-H attraction and an H-P repulsion as assumed in the model.

Altogether, the heteropolymer Hamiltonian writes as

$$H = \sum_{i=1}^L \frac{p_{x,i}^2 + p_{y,i}^2}{2m} + \sum_{i=1}^{L-1} V_1(r_{i,i+1}) + \sum_{i=2}^{L-1} V_2(\theta_i) + \sum_{i=1}^{L-2} \sum_{j=i+2}^L V_3(r_{ij}, \xi_i, \xi_j) \quad (5)$$

where all monomers are assumed to have the same mass m and momenta are defined as $(p_{x,i}, p_{y,i}) := m(\dot{x}_i, \dot{y}_i)$.

Accordingly, each heteropolymer is perfectly identified by a binary sequence of 0s and 1s specifying the nature of each monomer. Those sequences for which the heteropolymer shape converges systematically (at intermediate temperatures) towards the same ‘‘native’’ configuration independently of the initial condition are identified as ‘‘good folders’’. Previous studies, mostly based on Monte Carlo techniques indicate that this happens only in a few cases [11, 12, 13] and the scenario has been confirmed also by molecular dynamics simulations [9].

In what follows, we shall limit our investigations to the three following cases, all of length $L = 20$,

- [S0]=[0000 0000 0000 0000 0000] a homopolymer composed of hydrophobic residues only;
- [S1]=[0001 0001 0001 1001 1000] a sequence first studied in [12] (therein indicated with the code number 81) where it was identified as a good folder;
- [S4]=[1110 0100 0000 0001 0010] a randomly generated sequence with 6 P-type residues, identified as a bad folder in [9].

A reasonably accurate characterization of each sequence can be obtained by determining three transition temperatures. The first one, T_θ , denotes the temperature below which the polymer is in a collapsed rather than in a random-coil configuration [1]. It can be determined by studying the temperature dependence of the gyration radius $R_{gy}(T)$: T_θ corresponds to the maximum of $\partial R_{gy}(T)/\partial T$.

The folding temperature T_f is the temperature below which the heteropolymer stays predominantly in the native valley. Here, analogously to [9], we define the native valley as the basins of attraction of the NC and of its neighbouring minima. A quantitative estimate of T_f can be then obtained by determining the temperature at which the chain spends 50% of the time within the native valley.

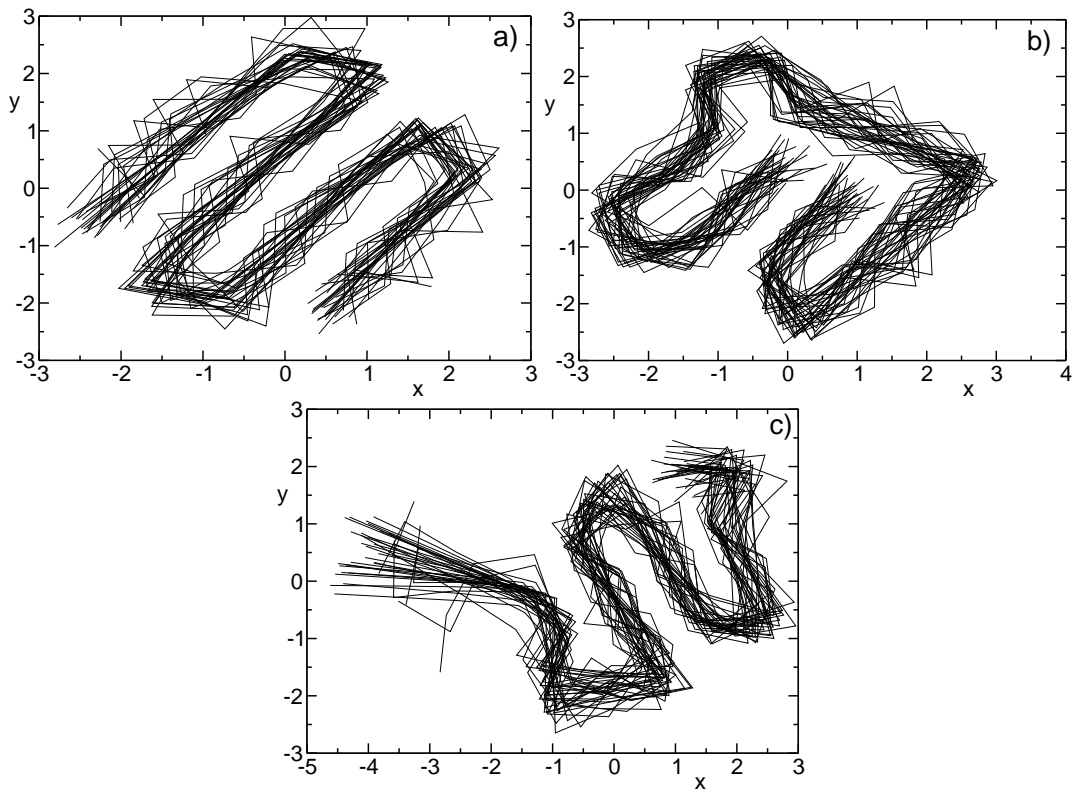


FIG. 1: Configurations of all the NNMs for the three considered sequences : S0 (a), S1 (b) and S4 (c).

Finally, the glass-transition temperature T_g can be identified by comparing (finite) time averages performed starting from different initial conditions. Specifically, we have considered unfolding (USs) and folding (FSs) simulations, whose initial conditions correspond to the NC and to random coil configurations, respectively. In practice, T_g is defined as the temperature below which the relative difference between USs and FSs averages of the internal energy U is larger than 10%.

We have determined T_θ , T_f , and T_g , by means of molecular-dynamics simulations with each monomer being in contact with a stochastic thermal reservoir at temperature T

$$\dot{z}_i(t) = p_{z,i}/m \quad ; \quad \dot{p}_{z,i}(t) = -\frac{\partial H}{\partial z_i} - \gamma p_{z,i}(t) + \eta_{z,i}(t) \quad (6)$$

Here z_i is introduced as a shorthand notation for both the spatial coordinates x_i and y_i , γ is the dissipation rate and $\eta_{z,i}(t)$ is a Gaussian distributed, δ -correlated random noise

$$\langle \eta_{z,i}(t) \eta_{z,j}(0) \rangle = 2\gamma m k_B T \delta(t) \delta_{i,j}, \quad (7)$$

where, k_B denotes the Boltzmann constant and T is the temperature (for the sake of simplicity, both k_B and m have been set to unit).

The temperature values obtained for $S0 - S1 - S4$ are reported in Tab. I, together with the number n_0 of the minima directly connected with the NC. The glassy transition has been determined by performing averages over a time lapse on the order of 10^6 units. These results are very close to those reported in [9], where a deterministic Nosé-Hoover thermostating scheme [14] was used instead. The advantage of using the Langevin equation (6) is that the damping rate can be directly controlled. As we shall see in the next section, this is a crucial ingredient for characterizing the escape rate from a given valley.

A more detailed characterization of heteropolymer dynamics can be obtained by identifying at least the most visited minima of the potential energy $V = V_1 + V_2 + V_3$. Here, we have proceeded by sampling a generic trajectory at time intervals of length $\Delta t \sim 1 - 5$. Then, the resulting instantaneous configurations have been taken as initial conditions for the overdamped dynamics

$$\dot{z}_i = -\frac{\partial H}{\partial z_i} \quad , \quad (8)$$

TABLE I: The collapse-transition temperature T_θ , the glassy temperature T_g , the folding temperature T_f , the number n_0 of nearest neighbour minima of the NC for the sequences S0 (homopolymer), S1 (good folder) and S4 (bad folder)

	S0	S1	S4
T_θ	0.16	0.11	0.13
T_g	0.022	0.048	0.025
T_f	0.044	0.061	0.044
n_0	31	37	36

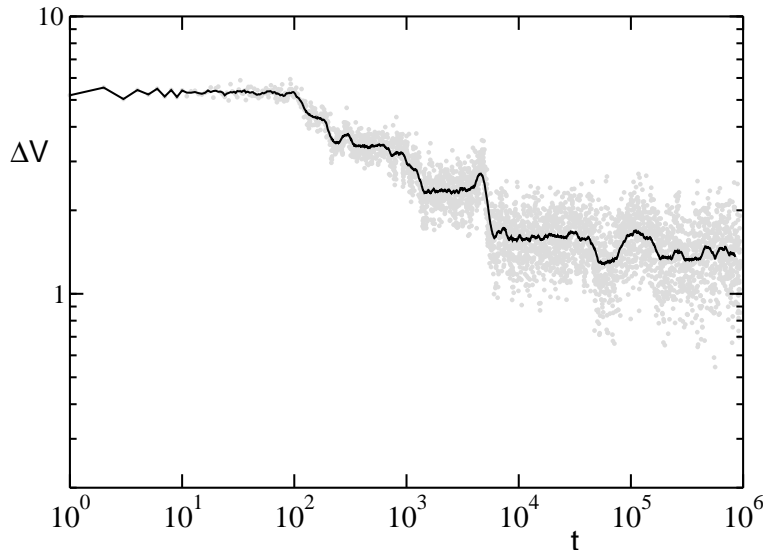


FIG. 2: Potential energy versus time during a folding simulation for the sequence S1 at $T = 0.055$ (grey circles). The solid line is a local average with exponentially increasing window size.

which drives the system to the minimum energy state, whose basin of attraction contains the initial condition [3]. The minima separated from the absolute minimum (the NC) by a single energy barrier have been denoted as nearest neighbouring minima (NNM), while those separated from the NC by two barriers as second-nearest neighbouring minima (2NNM), and so on. The NNM configurations for all the three examined sequences are reported in Fig. 1. Before passing to a specific discussion of the escape from a given valley, it is convenient to illustrate the outcome of a typical FS in the temperature range $T_g < T < T_\theta$. The evolution of the difference ΔV between the instantaneous potential energy and the potential energy V_0 of the NC is reported in Fig. 2 for the heteropolymer S1. A series of sudden conformational changes are clearly identifiable from the various energy drops (notice the logarithmic scale of both axes). Once S1 enters the native valley, it remains there for a very long time, although jumps towards neighbouring minima can occasionally occur.

III. ESCAPE RATE FROM A METASTABLE STATE

Since the publication of the pioneering paper of Kramers [15], the problem of determining the escape rate from a metastable state has been addressed in many different contexts. Here, we consider the overdamped dynamics of an ensemble of N interacting particles in a 2d environment. We restrict our discussion to the overdamped limit, since it is expected that in the protein folding problem, the time scale of energy exchanges with the thermal bath (through collisions with water molecules) is rather fast (we shall anyway return to this point later on). The probability density $P(\mathbf{r}, t)$ for a configuration to be in an infinitesimal volume around the state $\mathbf{r} \equiv (r_1, \dots, r_{2N}) = (x_1, y_1, x_2, \dots, x_N, y_N)$ at time t satisfies the Fokker-Planck equation

$$\frac{\partial P}{\partial t} = \frac{1}{\gamma m} \sum_{i=1}^{2N} \frac{\partial}{\partial r_i} \left(\frac{\partial V(\mathbf{r})}{\partial r_i} P + k_B T \frac{\partial P}{\partial r_i} \right), \quad (9)$$

where $V(\mathbf{r})$ represents the energy potential. The above is nothing but a continuity equation, with the r.h.s. representing the divergence of the probability flux

$$J_i \equiv -\frac{1}{\gamma m} \left[\frac{\partial V(\mathbf{r})}{\partial r_i} + k_B T \frac{\partial}{\partial r_i} \right] P(\mathbf{r}, t) = -\frac{k_B T}{\gamma m} \exp\left(\frac{-V(\mathbf{r})}{k_B T}\right) \frac{\partial}{\partial r_i} \left[\exp\left(\frac{V(\mathbf{r})}{k_B T}\right) P(\mathbf{r}, t) \right]. \quad (10)$$

The stationary solution (with no flux boundary conditions, $J_i = 0$) is simply given by $P(\mathbf{r}) = \exp[V(\mathbf{r})/(k_B T)]$. Let us now assume that the energy landscape exhibits at least two local minima m_a and m_b with energies respectively equal to V_a and V_b : we want to estimate the escape rate from the basin of attraction of m_a . The boundary separating the basins of attractions of the two minima coincides with the stable manifold of possibly more than one saddle point. Let us denote the energy on the saddle with \mathbf{r}_s is V_s . If the system is prepared into the state m_a , a flux \mathbf{J} sets in: if the flux itself is weak, it is basically constant in time and one can approach the problem by determining the stationary state with \mathbf{J} being a solenoidal field. Once \mathbf{J} is given, the escape rate Γ can be obtained by integrating the outgoing flux over the whole boundary of the well. We are not aware of a general solution in more than one dimension.

The most general case amenable to an analytic treatment is that of a potential which, in the vicinity of the saddle point, can be separated into two distinct contributions

$$V(\mathbf{r}) - V_s = V_{\parallel}(r_{\parallel}) + V_{\perp}(\mathbf{r}_{\perp}) \quad , \quad (11)$$

where r_{\parallel} is the distance from the basin boundary (measured along the unstable manifold of the saddle), while the vector \mathbf{r}_{\perp} parametrizes all other directions in phase space. Finally, the zeroes of V_{\parallel} and V_{\perp} are set in the saddle point. Under the above assumptions, the only nonzero component of the flux is

$$J_{\parallel} = -\frac{k_B T}{\gamma m} \exp\left(\frac{-V(\mathbf{r})}{k_B T}\right) \frac{\partial Q}{\partial r_{\parallel}} \quad (12)$$

where we have introduced $Q(\mathbf{r}) = \exp(V/k_B T)P(\mathbf{r})$ and J_{\parallel} depends only on r_{\parallel} . The vanishing of J_{\perp} implies that Q depends only on r_{\parallel} . Accordingly, Eq. (12) can be solved to yield

$$Q(r_{\parallel}) = \frac{1}{C} \int_{r_{\parallel}}^{r_s} e^{\frac{V_{\parallel}(\xi)}{k_B T}} d\xi \quad (13)$$

where the integration constant is determined by imposing that $Q(\mathbf{r})$ and, accordingly, $P(\mathbf{r})$ vanish along the boundary. The multiplicative constant C can be finally determined by normalizing the integral of $P(\mathbf{r})$:

$$C = e^{-\frac{V_a}{k_B T}} \int e^{-\frac{V(\mathbf{r})-V_a}{k_B T}} d\mathbf{r} \int_{r_{\parallel}}^{r_s} e^{\frac{V_{\parallel}(\xi)}{k_B T}} d\xi \quad . \quad (14)$$

The first integral is restricted to the basin of attraction of m_a . In the small temperature limit, in the region where $e^{-\frac{V(\mathbf{r})-V_a}{k_B T}}$ is significantly different from 0, the last integral is basically constant, so that we can replace its lower border with r_a , thus writing

$$C = e^{-\frac{V_a}{k_B T}} I_a I_{\parallel} \quad (15)$$

where

$$I_a = \int e^{-\frac{V(\mathbf{r})-V_a}{k_B T}} d\mathbf{r} \quad (16)$$

$$I_{\parallel} = \int_{r_1}^{r_s} e^{\frac{V_{\parallel}(\xi)}{k_B T}} d\xi \quad (17)$$

The flux then writes

$$J_{\parallel} = \frac{k_B T}{\gamma m} \frac{e^{-\frac{\Delta V}{k_B T}}}{I_a I_{\parallel}} e^{-\frac{V_{\perp}}{k_B T}} \quad (18)$$

where $\Delta V = V_s - V_a$. By integrating on the basin boundary, one finally obtains

$$\Gamma = \frac{k_B T}{\gamma m} \frac{I_{\perp}}{I_a I_{\parallel}} e^{-\frac{\Delta V}{k_B T}} \quad (19)$$

where

$$I_{\perp} = \int e^{-\frac{V_{\perp}(r_{\perp})}{k_B T}} dr_{\perp} \quad (20)$$

Eq. (19) holds under the assumption of a sufficiently small temperature ($\Delta V > k_B T$) and the separability condition (11). The former hypothesis is needed to ensure a sufficiently slow flux to guarantee that a quasi-stationary approach holds and the integral in Eq. (14) factorizes. The latter hypothesis ensures that Eq. (13) indeed represents a meaningful solution of the problem. One should notice that separability is required to hold only in the region around the saddle where the integral I_{\perp} has to be performed.

If the temperature is small enough, only the leading quadratic terms are relevant in the computation of the integrals I_a , I_{\parallel} and I_{\perp} . In this harmonic limit, they reduce to Gaussian integrals that can be computed by diagonalizing the Hamiltonian. Upon denoting with $\omega_a^{(i)}$ the $2N$ frequencies in the vicinity of the minimum m_a ($[\omega_a^{(i)}]^2 = -\Lambda_a^{(i)}/m$, $\Lambda_a^{(i)}$ being the negative i th eigenvalue of the Hessian), with $\omega_{\perp}^{(i)}$ the $2N - 1$ frequencies around the saddle (those corresponding to the stable directions), and with ω_{\parallel} the rate associated to the only expanding direction ($[\omega_{\parallel}]^2 = \Lambda_s^{(2N)}/m$), one obtains the expression first derived by Langer in 1969 [7, 16] [17].

$$\Gamma_L = \frac{\omega_{\parallel}}{\pi\gamma} \frac{\prod_{i=1}^{2N} \omega_a^{(i)}}{\prod_{i=1}^{2N-1} \omega_{\perp}^{(i)}} e^{-\frac{\Delta V}{k_B T}} \equiv \frac{\omega_{\parallel}^2}{\pi\gamma R} e^{-\frac{\Delta V}{k_B T}}, \quad (21)$$

where $R := \sqrt{\prod_{i=1}^{2N} |\Lambda_s^{(i)}| / \prod_{i=1}^{2N} |\Lambda_a^{(i)}|}$, can be interpreted as an entropy factor [18, 19]. In the case of continuous symmetries (as, e.g., translational and rotational symmetries), Hessian eigenvalues corresponding to Goldstone modes vanish. They have to be excluded in the frequency products appearing in Eq. (21) [16].

Expression (21) is routinely employed in studies of many-body systems, including relaxation dynamics in glasses [18] and in the estimation of entropy barriers in clusters [19]. However, its validity range has not been thoroughly investigated. For instance, in Ref. [20] a Master equation is constructed for a cluster of 19 atoms by identifying directly minima and saddles, but estimating transition probabilities only from an expression similar to Eq. (21).

In the weak damping limit, Eq. (21) generalizes to [21]

$$\Gamma_L = \frac{\zeta \omega_{\parallel}^2}{\pi\gamma R} e^{-\frac{\Delta V}{k_B T}}, \quad (22)$$

where the multiplicative correction

$$\zeta = \frac{2}{1 + \sqrt{1 + (2\omega_{\parallel}/\gamma)^2}}, \quad (23)$$

depends on the ratio between the damping constant and the divergence rate along the expanding direction.

Finally, we mention a simplified formula for the escape rate that is somehow halfway between the general expression (19) and that one corresponding to the linearization (21). Under the hypothesis of a fully separable potential, one can factorize the two integrals I_a and I_{\parallel} into products of one-dimensional integrals

$$I_a = \prod_{i=1}^{2N} \int e^{-\frac{V_i(r_i)}{k_B T}} dr_i \quad (24)$$

$$I_{\parallel} = \prod_{i=1}^{2N-1} \int e^{-\frac{V^{(i)}(r^{(i)})}{k_B T}} dr^{(i)} \quad (25)$$

where V_i is the i th component of the potential in the vicinity of the minimum with the zero of the scale such that $V_i(0) = 0$, and $V^{(i)}$ is the analogous around the saddles for the stable directions.

In the following section we compare Langer prediction (21) with our numerical results. In Sect. V we discuss the limits of applicability of Eq. (21) and we test the improved expression for the escape rate (19) (with the integrals estimated as in Eqs. (24,25)).

IV. NUMERICAL RESULTS

In order to characterize the dynamics of the polymer in the native valley we have determined both analytically and numerically the escape rate from the NC towards any of the NNMs. The procedure for identifying the NNMs from a database of ‘‘inherent’’

minima, constructed by following the method outlined in Sect. II, relies on the identification of the minimal energy path connecting each NNM to the NC. The algorithm used to find these paths is described in the Appendix: it allows identifying the saddle separating any two minima.

A few pairs of NNMs turn out to be connected by more than one (up to 3) minimal energy path, this implying that they are separated by more than one saddle. In these cases, one should, in principle, compare the numerically determined escape rate with the sum of the probability flows Γ_L through the different saddles. As a matter of fact, we limited to consider the contribution of the saddle yielding the maximal flow. This approximation is definitely negligible with respect to the discrepancies between numerical and theoretical estimates fully discussed in the following.

In Fig. 3 the three potential contributions V_1 , V_2 , and V_3 are reported for a minimal energy path connecting the NC to one of the NNMs. A common feature to all the examined paths is that the main contribution to the potential energy barrier arises from the Lennard-Jones term. This confirms that the term driving the folding is indeed the long-range potential term mimicking the hydrophobicity effects (as already mentioned in [9]).

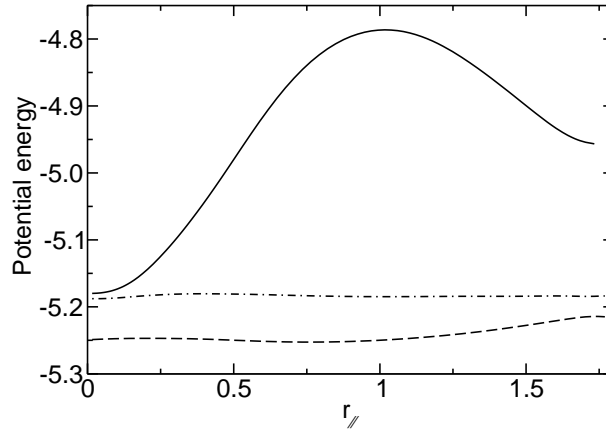


FIG. 3: Potential energy profiles versus the distance from the NC (measured along the unstable manifold of the saddle) r_{\parallel} . The three curves correspond to the different potential contributions for a minimal energy path connecting the NC to a nearest neighboring minimum for the sequence S1. The solid line indicates the Lennard-Jones contribution V_3 (4), while the dashed line the harmonic term V_1 (1) and the dot-dashed line the potential term V_2 (2). The last two terms are shifted along the vertical axis by a factor -5.2 and -5.75 , respectively.

The evaluation of Γ_L requires the knowledge of the eigenvalues of the Hessian in both the NC and a suitable saddle. In our model, because of translational and rotational symmetries, three eigenvalues always vanish. This is clearly seen in Fig. 4, where the frequency spectrum $\omega_a^{(i)}$ of the NC is plotted for the three sequences (panel a), together with the spectrum $\omega_{\perp}^{(i)}$ of one saddle (panel b). The $\omega_a^{(i)}$ spectrum decreases smoothly from values around 13 down to 0. It is interesting to notice that all spectra do not differ significantly from what one would obtain for a purely harmonic chain, in which case the spectrum would decrease from a maximum frequency equal to $2\sqrt{2\alpha} = 12.6$ down to zero. It is only at lower frequencies that differences among the various sequences can be appreciated: in fact, this spectral band is basically determined by the angular motion that is primarily controlled by the cosine (2) and Lennard-Jones (4) potentials.

For what concerns the value of ω_{\parallel} , it turns out to range between 0.3 and 1.8 in all saddles.

Then, we have directly determined the escape rate $\Gamma(j)$ from the NC by performing several USs with the damping constant set equal to 6.9. Every Δt time units, the “inherent” polymer configuration is determined by a steepest descent method. As soon as the polymer leaves the basin of attraction of the NC, the corresponding time is registered together with the new minimum that has been reached. Let us denote with M_j the number of USs ending in the j -th minimum, with $\langle \tau_j \rangle$ the corresponding average escape time and with $M = \sum_{j=1}^{n_0} M_j$ the total number of USs. We have verified that $\langle \tau_j \rangle$ is independent of j . This indicates that the polymer spends most of the time before any jump in exploring the same region in the phase space, consistently with the hypothesis of a thermally activated process. Thus, the escape rate toward the j -th minimum can be numerically estimated as

$$\Gamma(j) = \frac{M_j}{M} \frac{1}{\langle \tau \rangle}, \quad (26)$$

where we have dropped the dependence on j in the escape time.

We have focused our numerical analysis in the temperature range $[T_g, T_{\theta}]$, where the polymer spends most of the time in a collapsed state. In order to obtain a sufficient statistics the parameters of USs have to be suitably tuned according to the temperature values. In particular, the sampling time Δt has to be maintained sufficiently short to avoid back-crossings of the barrier and multiple jumps. More precisely, it must be smaller than the lifetime of all NNMs. Since all lifetimes decrease with

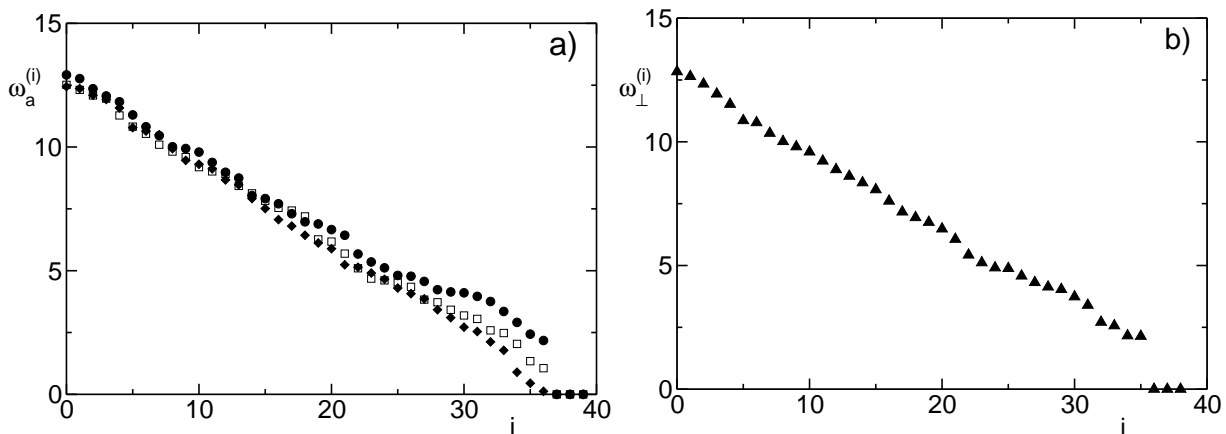


FIG. 4: a) Angular frequencies $\omega_a^{(i)}$ associated to the Hessian of the NC for the sequence S0 (squares), S1 (circles) and S4 (diamonds); b) angular frequencies $\omega_\perp^{(i)}$ associated to the Hessian of a saddle separating the NC from a NNM for the sequence S1.

the temperature, increasingly smaller Δt 's have to be adopted when the temperature is increased [22]. We have chosen Δt -values ranging from 1 at low temperatures ($T \simeq T_g$), to 10^{-3} at high temperatures ($T \simeq T_\theta$), while the integration time step has been kept equal to 10^{-3} (a few tests performed with an integration time step $\simeq 10^{-4}$ have not revealed any relevant difference). Anyway, at low temperatures the escape rate towards a subset of NNM is so small that in practice they are never found to be visited over an extremely large number of simulations. This is why in Table II we indicate the number n_v of visited NNM as a function of the temperature: it turns out that all NNM are visited already at $T = 0.08$ for both S0 and S1, while for S4 new minima are found up to $T = 0.1$ (the highest temperature we have examined).

The numerically computed transition rates are presented in Fig. 5, where only the results for the most visited NNMs are reported (see the dashed lines). The solid lines refer to the theoretical estimates. We expect that Eq. (21) holds, since the chosen value of the damping coefficient, $\gamma = 6.9$, should guarantee an overdamped dynamics.

While at $T \simeq 0.04$, the analytic expression Γ_L is in good agreement with the numerical estimates (for all of the three sequences), at higher temperatures the theoretical expression overestimates the escape rate. In order to perform a quantitative comparison, it is convenient to compute the ratio

$$r_j = \frac{\Gamma_L(j)}{\Gamma(j)} \quad , \quad (27)$$

for each escape process towards an NNM and to then average over all neighbouring minima

$$\langle r \rangle = \sum_j P_j r_j \quad , \quad (28)$$

where $P_j = \Gamma(j) / \sum_i \Gamma(i)$ is the probability that an US ends up in the j -th NNM and the sum is restricted to those minima that have been visited at least twice. The values of $\langle r \rangle$ for the three sequences at four different temperatures from 0.04 up to 0.1 are reported in Tab. II. In this range, statistically reliable estimates are obtained already for $M > 10^3$. In all cases, the theoretical formula is reasonably accurate at low temperatures, but it downgrades when going above the ‘‘folding’’ temperatures and the phenomenon is more evident in the case of the good folder S1.

V. DISCUSSION OF THE RESULTS

In this section we discuss several independent factors that can a priori affect the observed escape rates. First of all, we have investigated whether intrinsic fluctuations due to the chaotic dynamics contribute significantly to the escape rates. In order to examine this point, we performed microcanonical simulations at various temperatures (namely $T = 0.04, 0.06$, and 0.08). Although the potential energy is larger than the barrier height, no jumps have been observed in simulations lasting up to $2 \cdot 10^6$ time units. This means that local fluctuations are not strong enough to trigger jumps between neighbouring valleys in the presence of a global energy conservation. Therefore, fluctuations due to the coupling with independent heat baths are a crucial ingredient in establishing the time scale of the escape rate.

Yet the observed discrepancy between the analytic expression (21) and the numerically evaluated escape rate calls for an explanation. Eq. (21) has been derived by making several assumption that may not be fulfilled in practice:

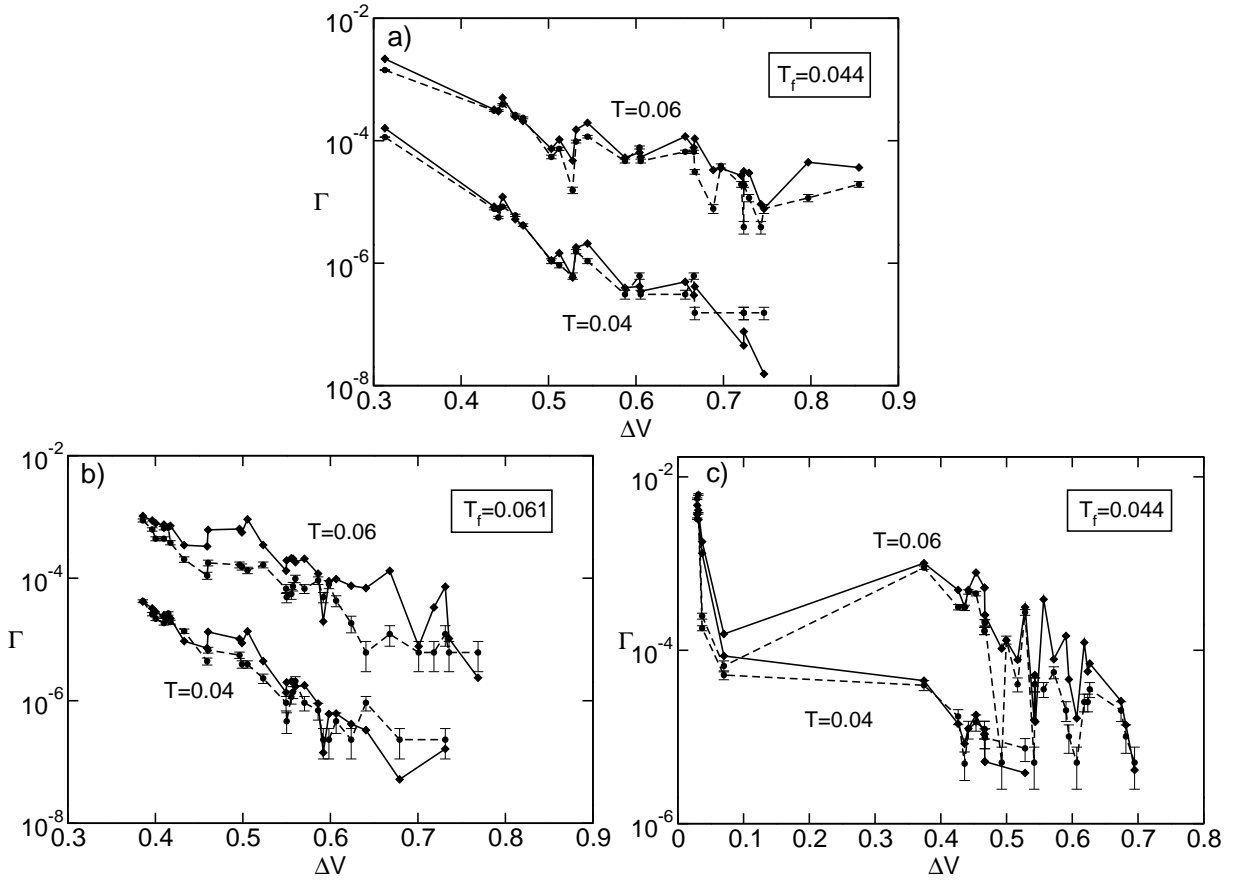


FIG. 5: Transition rates Γ versus the barrier height ΔV : comparison of the theoretical expression (21) (solid line) with the numerical estimate (26) (dashed line) for two different temperatures ($T = 0.04$ and $T = 0.06$) for the three studied sequences. Namely, (a) S0; (b) S1 and (c) S4. The numerical data refer to a total number $M = 1,000 - 5,000$ of USs and to a sampling time $\Delta t = 1$.

1. the value of the friction coefficient γ should be larger than the frequency associated to the expanding direction of the saddle ω_{\parallel} , i.e. the dynamics should be overdamped;
2. the configurational probability density $P(\mathbf{r}, t)$ should be almost stationary, i.e. the polymer should be well thermalized before a jump occurs;
3. the potential energy should be well approximated by the quadratic contributions in the relevant regions around both the saddles and the NC;

In the following we investigate the validity of these assumptions.

A. Overdamped Limit

Throughout this paper we have fixed γ equal to 6.9 in adimensional units. In order to check whether this is a meaningful choice in the protein context, we must express the damping rate in physical units, $\gamma = 6.9m/\tau_o$, where m is the mass of a typical aminoacid, while τ_o is the period of small oscillations within the potential well. Since $m \sim 10^{-22}$ g and $\tau_o \sim 10^{-12}$ s, it follows that $\gamma \sim 10^{-9}$ g/s, a value to be compared with the typical relaxation rate due to collisions with water molecules $\gamma_{H_2O} \simeq 10^{-8} - 10^{-9}$ g/s (see Ref. [23] for a more detailed discussion). Our choice of γ is, therefore, not too far from reality. Moreover, since γ is already four times larger than the maximum ω_{\parallel} , we expect the system dynamics to be in the overdamped regime.

Anyhow, it is instructive to investigate whether the damping rate is responsible for the non perfect agreement between numerical data and the approximate theoretical expression. In order to clarify this point we performed further USs with both a smaller ($\gamma = 1$) and a larger ($\gamma = 49$) friction. Since γ , in the former case, is of the order of ω_{\parallel} , one should merely expect multiplicative corrections arising from the ζ/γ factor in Eq. (22). By neglecting saddle-to-saddle fluctuations of ω_{\parallel} (assumed always equal to

TABLE II: For all the sequences and four different temperatures T we report: the numerically estimated average escape time $\langle\tau\rangle$, the number of visited NNM n_v (the numbers within brackets refer to the minima visited more than once) and the weighted ratio $\langle r\rangle$.

T	$\langle\tau\rangle$	n_v	$\langle r\rangle$
S0 - 0.04	6484	20(16)	1.37
0.06	265	27(25)	1.42
0.08	42	31(30)	1.76
0.10	19	31(30)	3.43
S1 - 0.04	4375	28(23)	1.31
0.06	168	32(27)	1.95
0.08	24	37(34)	2.05
0.10	19	37(36)	3.89
S4 - 0.04	129	12(11)	1.30
0.06	58	28(24)	1.42
0.08	30	27(25)	2.16
0.10	18	30(24)	3.74

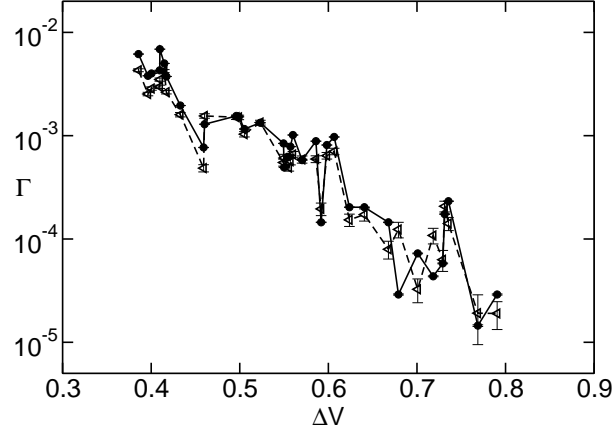


FIG. 6: Numerical transition rates Γ vs. the barrier height ΔV for two different γ -values. Filled circles refer to $\gamma = 1$, while empty triangles correspond to $\gamma = 49$. The latter have been scaled by a factor 49×0.56 (see text). Simulations refer to sequence S1 at $T = 0.07$. The number of USs is $M \simeq 4,000$.

its average value 1.17), this amounts to a correction term 49×0.56 . In Fig. 6, we have multiplied by this factor the numerical data obtained for $\gamma = 49$. The quite good overlap between the two sets of data confirms that the dependence on the damping term is well reproduced by the theoretical formula (part of the oscillations is of statistical nature and part is due to the neglected ω_{\parallel} fluctuations).

B. Thermalization time

A fundamental hypothesis implicitly made in the derivation of the analytical expression for the escape rate is that the probability density of initial conditions inside the native valley can be approximated by the product of the Boltzmann-Gibbs distribution times a factor that differs significantly from 1 only in the neighborhood of the saddle. In order to verify the validity of this assumption, we have studied the decay of the autocorrelation functions for the kinetic and potential energy in several USs with S0 and S1.

From the data reported in Tab. III, it is evident that the typical correlation times are much smaller than the average escape times at all the examined temperatures. Since the correlation time is a reasonable estimate for the time required to reach a “local thermal equilibrium”, these results suggest that, whatever the distribution of initial condition used for the USs is, the system thermalizes before escaping. In fact, USs performed by starting from different sets of initial conditions lead to close Γ values.

TABLE III: Decay times for the autocorrelation function of the kinetic energy τ_K and potential energy τ_V , for S0 and S1 at various temperatures T . The times $\tau_{K,V}$ are estimated by assuming an exponential decay for the autocorrelation functions. The functions has been obtained by averaging over $M = 10$ different USs.

T	τ_K - S0	τ_V - S0	τ_K - S1	τ_V - S1
0.02	0.13	0.70	0.10	0.65
0.04	0.12	1.16	0.10	0.95
0.06	0.14	2.17	0.10	1.55
0.08	0.13	2.66	0.10	1.52

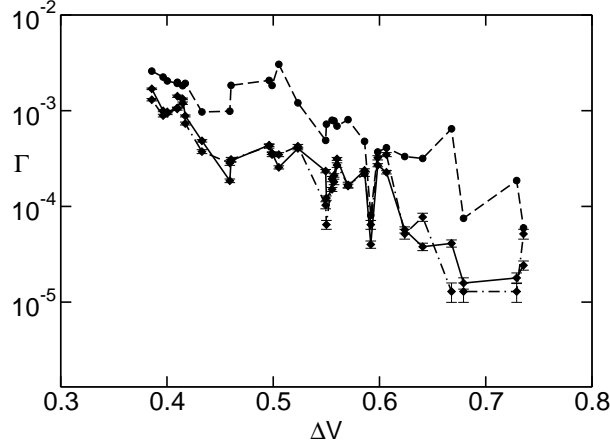


FIG. 7: Transition rates Γ versus the barrier height ΔV . Langers's expression (21) (dashed line) is compared with the numerical estimate for two choices of initial conditions: with (dot-dashed line) and without (continuous line) thermalization. Data refers to the sequence S1 at temperature $T = 0.07$ with $M = 1,000$ and a thermalization time $T = 100$.

For instance, in Fig. 7 one can compare the results of simulations started from a Maxwellian distribution of the velocities (dot-dashed line) with those obtained by gradually warming (with a 7×10^{-4} rate) an initially frozen configuration. The relative differences are much smaller than the deviations from the theoretical expectation (dashed line).

However, Tab. III brings forth some interpretative problems: while the correlation time of the kinetic energy does not depend on T and is proportional to the friction coefficient, the correlation time of the potential energy $V(t) = V_1(t) + V_2(t) + V_3(t)$ decreases with temperature. This phenomenon can be directly observed in Fig. 8, where the absolute value of $C(\tau) = \langle V(t)V(t+\tau) \rangle$ is plotted for different temperatures. The partial slowing down is an entirely nonlinear effect, since no temperature dependence can arise in a purely harmonic potential. In the next subsections we shall see that nonlinearities are indeed at the origin of the limited validity of the theoretical formula.

C. Role of nonlinearities

Langer's estimate assumes that the potential is harmonic in the vicinity of both the NC and the saddle. In order to test whether nonlinear corrections may be important, we have estimated expression (19) under the hypothesis of a fully separable potential. In fact, from the products of the one-dimensional integrals in Eqs. (24,25), one can at least establish whether nonlinear corrections are truly important. In practice, we have evaluated the integrals along the eigendirections of the Hessian in the NC and in the corresponding saddle. The integration interval for the i -th eigendirection is set equal to $[-r_i^*, r_i^*]$, where $r_i^* = 3\sqrt{2\pi T/\omega_a^{(i)}}$ for I_a and analogously $r_i^* = 3\sqrt{2\pi T/\omega_\perp^{(i)}}$ for I_\perp .

The comparison of this expression with both numerical results and the standard Langer's formula is presented in Fig. 9 for the sequence S0. Although there is no reason to expect the potential to be separable, it is interesting to notice that the refined theoretical expression improves over Langer's formula. On the other hand, the remaining sizeable deviations from the numerical results indicate the need of a really improved theoretical formula.

The derivation of Langer's formula reveals that an activation process can be decomposed into an Arrhenius factor, controlled

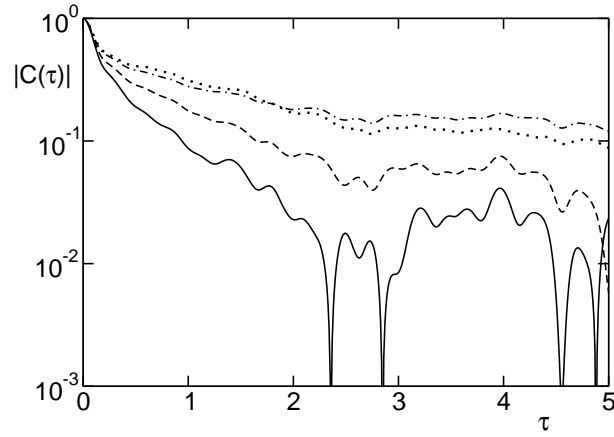


FIG. 8: Initial decay of the absolute value of the autocorrelation function $C(\tau)$ for the potential energy during canonical simulations at $T = 0.02$ (continuous line), $T = 0.04$ (dashed line), $T = 0.06$ (dot dashed line), $T = 0.08$ (dotted line). For each temperature $C(\tau)$ is averaged over a time span of 50 and over 10 different trajectories.

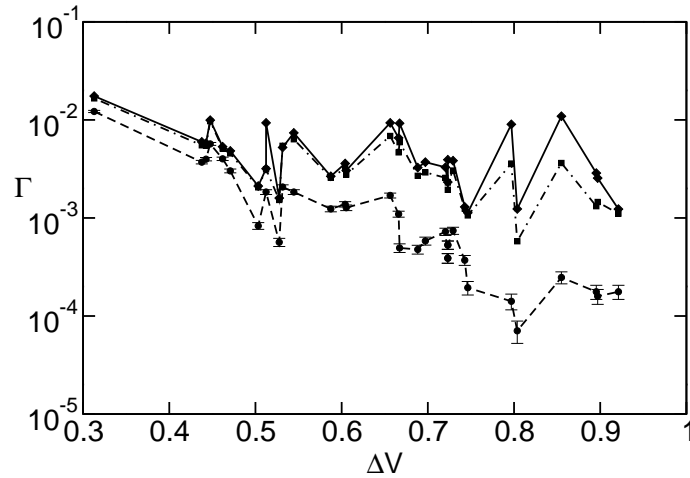


FIG. 9: Transition rate Γ versus the barrier height: comparison of Langer's expression (21) (solid line) with numerical estimate (26) (dashed line) and with expression (19) equipped with Eqs. (24,25) (dot-dashed line) for S0 at $T=0.1$. Numerical estimates have been obtained with a sampling time $\Delta t = 0.03$ and performing $N=3000$ USs.

by the energy difference ΔV , and an entropic factor R . The analysis of the latter one conveys useful information on the structure of the potential energy landscape and helps shedding some light on the above mentioned discrepancies. While, a priori, there is no reason to expect R to be either smaller or larger than 1, in practice, it is almost always smaller than 1 (see Fig. 10); the only exceptions are four saddles all around the energy minimum of S4, which are also characterized by extremely low barriers. In fact, such saddles are quite peculiar in that they almost coincide with the NC except for the first 3-4 beads, which are, on the other hand, relatively distant from the core of the configuration[24]. Similar distributions of R -values have been also found in small clusters of particles interacting through Lennard-Jones potentials [18, 19].

The presence of such large entropic factors accounts for the peculiar dependence of the escape rate on ΔV for S4. The abrupt drop of Γ when ΔV is decreased below 0.2 (see Fig. 5) is due to the smallness of the entropic contribution (Γ is inversely proportional to R). This interpretation is further confirmed by the slow dependence of Γ on the temperature for such saddles.

Leaving aside this peculiarity, there is an average tendency of R to decrease upon increasing the barrier height in both S0 and S4; this indicates that higher barriers correspond to flatter saddles and thereby can be more easily overcome. This is not the case of the good folder, where R does not show any clear trend and is always bounded in the interval $[10^{-2}, 10^{-1}]$. Accordingly, all the NNMs are entropically equivalent and the escape rate is essentially determined by the Arrhenius factor.

The most interesting observation can be, however, made by parametrizing the relative error e_j (see Eq. (27)) of the escape rate r_j towards the j th NNM. From Fig. 11, one can see that the deviation of Langer's formula becomes systematically larger

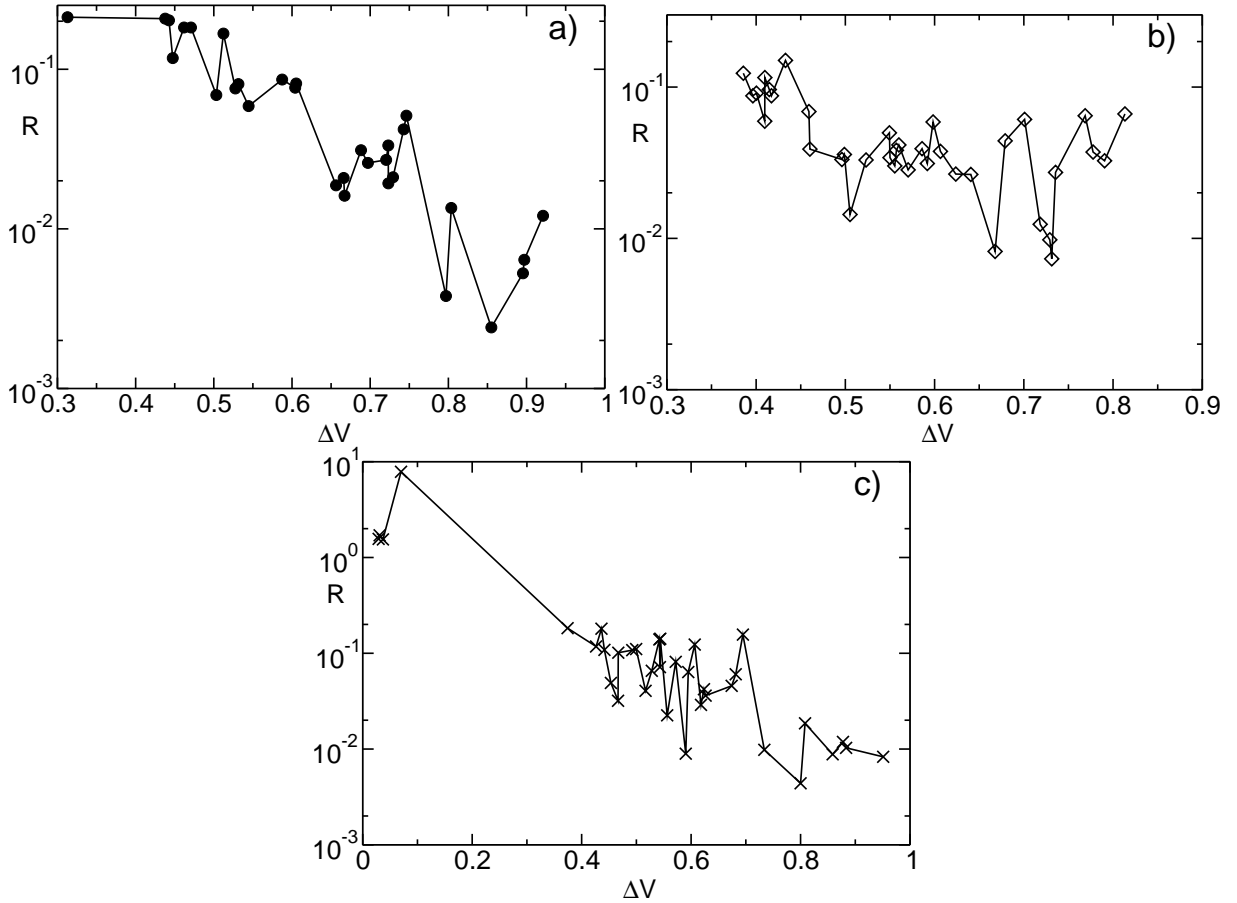


FIG. 10: Entropy ratios R versus the barrier height ΔV , for the three studied sequences: (a) S0 , (b) S1 and (c) S4.

upon decreasing R . This is qualitatively understandable, since a small R implies a flat saddle; therefore it is reasonable to expect nonlinear corrections to be more relevant. What is less obvious is the observed dependence of e_j on R . The data reported in Fig. 11 reveal that $e_j \approx a/R$, which amounts to conjecturing that $\Gamma \simeq 1/(R + a)$ with a basically independent of j . This is quite a remarkable result considering that the fit is more convincing at larger temperatures, when values as large as 60 of e_j are observed.

VI. CONCLUDING REMARKS

We have studied in detail the unfolding dynamics of short homo- and heteropolymeric chains made of N -beads in two dimensions. Polymers have been simulated via an off-lattice model previously introduced [8] and their evolution has been examined within the canonical ensemble. Our results suggest that the dynamics of polymers within their *native valley* can be described as a thermally activated process in a $2N$ -dimensional space in a whole range of temperatures above and below the folding temperature.

As a matter of fact, Langer's estimate for the escape rate represents a good approximation for all the examined sequences at low temperatures. We have verified that discrepancies between Langer's estimate and numerical data are mainly due to the poor approximation (limited to the harmonic terms) of the potential around the stationary points. A better estimate can be derived by taking into account higher order terms in the expansion of the potential. Since the folding temperatures for the homopolymer (S0) and the bad folder (S4) are relatively low, for these sequences the dynamics within the native valley can be reproduced reasonably well already with Langer's approximation. While for the good folder (S1), this is not the case, thus suggesting a more relevant role of nonlinearities at the folding temperature. In any case all the examined estimates turn out to be upper bounds for the escape rates.

An analysis of the entropic contribution to the escape rate suggests that the folding behaviour of a sequence can be related to topological properties of the landscape around the NC. For bad folders higher energy barriers are associated to flatter saddles, thus favouring jumps towards more unfolded configurations. On the other hand, for the good folder the entropy ratio seems not

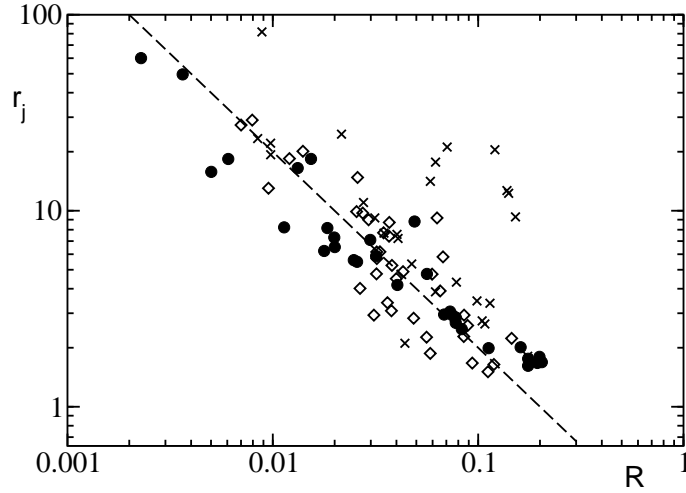


FIG. 11: The relative error e_j versus the entropic factor R for S0 (circles), S1 (diamonds) and S4 (crosses). The data have been obtained by sampling a trajectory every 0.3 time units at a temperature $T = 0.1$. The dashed line is a guide for the eye and it corresponds to a slope one.

to be related to the height of barriers.

We would like to stress that our analysis amounts to explore the free energy landscape of a polymer, since in the jumping rate estimates are included not only Kramers' terms but also entropic contributions. The relevance of the latter in determining equilibrium and kinetic properties of peptides has been recently pointed out in [5, 6].

In order to further explore the role of activation processes for the complete folding dynamics we plan to extend our analysis to the whole energy landscape. A complete graph describing all the folding/unfolding paths with their associated probabilities will allow to determine equilibrium properties of the system and possibly to distinguish bad and good folders.

Acknowledgments

We warmly acknowledge the active contribution given at the early stage of this work by Annalisa Tiberio[25]. We are also grateful to CINECA in Bologna and INFN for providing us access to the parallel computer CRAY T3E and to the Beowulf Linux-cluster under the grant "Iniziativa Calcolo Parallelo". This work has been partially supported under the FIRB project RBAU01BZJX "Dynamical and statistical analysis of biological microsystems".

APPENDIX A: ALGORITHM FOR THE IDENTIFICATION OF THE SADDLES

The algorithm described in this appendix (see also [25]) aims at determining the path of minimal potential energy connecting two minima indicated as \mathbf{a}_1 and \mathbf{a}_2 .

Due to the symmetries of the potentials defined in Section II (see eq. (5)), each spatial configuration of the polymeric chain is defined apart from a translation, a reflection and a rotation around an axis perpendicular to the xy -plane. Accordingly, after having expressed \mathbf{a}_1 in an arbitrary reference frame, it is convenient to determine the coordinates of \mathbf{a}_2 are by minimizing its Euclidean distance from \mathbf{a}_1 with respect to the above mentioned symmetry transformations.

The algorithm then consists in evolving a suitably chosen path connecting \mathbf{a}_1 and \mathbf{a}_2 according to a gradient dynamics until the maximum of the energy along the path converges to a minimum corresponding to a saddle. More precisely, the approach is split into three steps:

1. **Choice of the initial configurations** The initial path \mathcal{C}_0 connecting \mathbf{a}_1 and \mathbf{a}_2 is generally chosen by linearly interpolating between their coordinates,

$$\begin{aligned} x(i) &= x^1(i) + r(x^2(i) - x^1(i)) \\ y(i) &= y^1(i) + r(y^2(i) - y^1(i)) \\ i &= 1, \dots, N \end{aligned} \quad (\text{A1})$$

The sequence of initial configurations along the path C_0 is fixed by varying the parameter r between 0 and 1 (we typically choose $r = m/100, 0 \leq m \leq 100$).

2. Evolution of the configurations Each configuration is then let evolve according to the gradient dynamics

$$\begin{aligned}\dot{x}_i &= -\frac{1}{\tilde{\gamma}} \frac{\partial H}{\partial x_i} \\ \dot{y}_i &= -\frac{1}{\tilde{\gamma}} \frac{\partial H}{\partial y_i}\end{aligned}\quad . \quad (\text{A2})$$

In practice, the damping coefficient $\tilde{\gamma}$ can be chosen equal to one, since it only determines the evolution time scale. The integration time step δt is adapted to the instantaneous value of the force field, $\delta t = \min(.01, .01/F_{max})$, where $F_{max} = \max_i\{|f_i^x|, |f_i^y|\}$ while f_i^x and f_i^y are the x and y components of the force acting on the i th bead.

3. Interpolation phase After letting evolve the system for a time $\bar{t} = 10\delta t$, the Euclidean distance $\Delta_m(\bar{t})$ between the m th and the $(m+1)$ st point is computed. If $\Delta_m(\bar{t}) > 2\Delta_m(0)$, a new configuration, is added between the two points by linearly interpolating between them. If $\Delta_m(\bar{t}) < \Delta_m(0)/2$ the $(m+1)$ -st configuration is removed. In this way, we are able to work with a set of uniformly distributed configurations, without loosing resolution in the regions where the energy gradient is large.

The last two steps are repeated until F_{max} in the maximum energy configuration along the path becomes smaller than a fixed threshold typically chosen equal to 10^{-3} . The coordinates of the saddle point are finally refined by implementing a standard Newton scheme.

On one hand, the path connecting two generic minima can exhibit more than one relative energy maximum (see, e.g., Fig. 12): this is an indication that the two minima are not nearest neighbours. In this case, our approach allows identifying new minima. On the other hand, it can happen that neighbouring minima are separated by more than one saddle: upon choosing different initial paths, one can, in principle, identify all saddles. Our simulations suggest that multiple saddles are not very common at least in the vicinity of the NC.

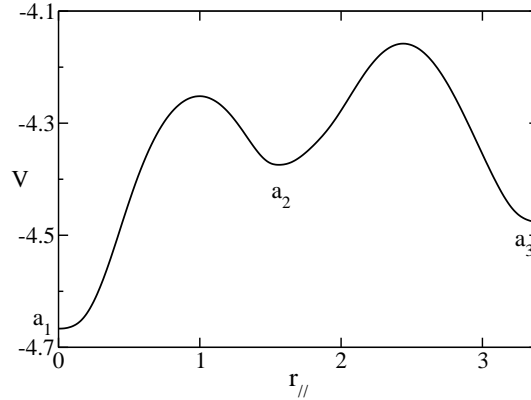


FIG. 12: Potential energy profile V connecting the NC \mathbf{a}_1 to a 2NNM \mathbf{a}_3 via 2 saddles for the sequence S1, the symbol \mathbf{a}_2 indicates a NNM. The index $r_{||}$ refers to the distance measured along the unstable manifold connecting the minima.

-
- [1] P.G. De Gennes, *Scaling Concepts in Polymer Physics* Cornell University Press, 1979, New York.
 - [2] T.E. Creighton, *Proteins: Structures and Molecular Properties* W.H. Freeman & Co., New York, 1993.
 - [3] F.H. Stillinger and T.A. Weber, *Science* **225** (1984) 983.
 - [4] R.S. Berry, N. Elmaci, J.P. Rose, and B. Vekhter, *Proc. Natl. Acad. Sci* **94** (1997) 9520.
 - [5] S.V. Krivov and M. Karplus, *J. Chem. Phys* **117** (2002) 10894.
 - [6] D.A. Evans and D.J. Wales, *J. Chem. Phys* **118** (2003) 3891.
 - [7] J.S. Langer, *Ann. Phys.* **54** (1969) 258.
 - [8] F.H. Stillinger, T.H. Gordon, and C.L. Hirshfeld, *Phys. Rev. E* **48** (1993) 1469.

- [9] A. Torcini, R. Livi, and A. Politi, *J. Biol. Phys.* **27** (2001) 181.
- [10] For the sake of simplicity, all variables are expressed in adimensional units. The harmonic term turns out to be stiff because $\alpha = 20$ is much larger than the constants corresponding to the two other interaction processes included in the model.
- [11] A. Irbäck and F. Potthast, *J. Chem. Phys.* **103** (1995) 10298.
- [12] A. Irbäck, C. Peterson, and F. Potthast, *Phys. Rev. E* **55** (1997) 860.
- [13] E. Marinari, and G. Parisi, *Europhys. Lett.* **19** (1992) 451.
- [14] S. Nosé, *J. Chem. Phys.* **81** (1984) 511; W.G. Hoover, *Phys. Rev. A* **31** (1985) 1695.
- [15] H.A. Kramers, *Physica* **7** (1940) 284.
- [16] J.S. Langer, *Ann. Phys.* **41** (1967) 108.
- [17] The original formula differs by a factor-2 since we are here referring to the first passage time at the boundary, rather than to the neighboring minimum.
- [18] L. Angelani, G. Parisi, G. Ruocco, and G. Vilianni, *Phys. Rev. Lett.* **81** (1998) 4648; *Phys. Rev. E* **61** (2000) 1681.
- [19] G. Daldoss, O. Pilla, G. Vilianni, C. Brangian, and G. Ruocco, *Phys. Rev. B* **60** (1999) 3200.
- [20] R.E. Kunz and R.S. Berry, *J. Chem. Phys.* **103** (1995) 1904.
- [21] P. Hänggi, P. Talkner, and M. Borkovec, *Rev. Mod. Phys.* **62** (1990) 251.
- [22] An upper bound for the lifetime τ_l of a NNM is given by the inverse of the escape rate from it to the NC evaluated by employing Eq. (21). With reference to temperatures in the interval $[0.02, 0.08]$, we have found $12 \leq \tau_l \leq 37$ for S0, $7 \leq \tau_l \leq 20$ for S1, and $0.06 \leq \tau_l \leq 1.06$ for S4.
- [23] T. Veitshans, D. Klimov, and D. Thirumalai, *Folding & Design* **2** (1997) 1.
- [24] Notice that the first three beads of S4 are all polar and are thus repelled by the vast majority of the remaining hydrophobic ones.
- [25] A. Tiberio, *Laurea Thesis* Università di Firenze, Firenze, 2000.